ORIGINAL PAPER

WPI and Cellulose Nanofibres Bio-nanocomposites: Effect of Thyme Essential Oil on the Morphological, Mechanical, Barrier and Optical Properties

Raissa Alvarenga Carvalho[1] · Ana Carolina Salgado de Oliveira[1] · Taline Amorim Santos[1] · Marali Vilela Dias[1] · Maria Irene Yoshida[2] · Soraia Vilela Borges[1]

Abstract

The uncertainty of consumers about the toxicological effects of synthetic antioxidants incorporated into the packaging has led to a demand for natural substituents that exhibit antioxidant activity without adding risk to the consumers. In this context, the effects of adding different concentrations of thyme essential oil (TEO) (20, 30, and 40% w/w) to whey protein isolate (WPI) and cellulose nanofibre (CNF) bio-nanocomposites developed by casting were studied. Scanning electron microscopy showed a reduction in the dispersion of CNF's in all films with the addition of TEO. The addition of TEO also decreased the water vapor permeability, increased the glass transition temperature, and crystallinity index. For the mechanical properties, the addition of TEO produced less rigid and elastic films with decreased in tensile strength, elongation at break, puncture strength, puncture deformation, and elastic modulus. In addition, the mechanical properties showed the formation of non-interactive systems and the FTIR spectra showed maintenance of the phenolic compounds of the TEO after the synthesis of the films. The optical properties showed that films were less yellow (b*) with a tendency to green (a*), less saturated (c*), and less transparent when compared with the control (0% TEO). The addition of TEO to bio-nanocomposites of WPI and CNFs, in the concentration range tested, enabled the formation of materials with properties that encourage the studies for various applications.

Keywords Packaging · Bio-nanocomposites · Essential oil · Characterization · Food application

Introduction

Packaging made from biopolymers found in nature, such as polysaccharides (starch, chitosan, galactomannan, and pectin) and proteins (caseinate, gelatin, and whey protein), has received great attention as alternatives to synthetic packaging produced from non-renewable resources, which are considered to be non-biodegradable [1–5].

Whey protein isolate (WPI) is a co-product of cheese or casein and has been extensively studied for the production of biodegradable packaging. Excellent results have been reported in terms of its role as an oxygen barrier and its film-forming capacity [6–9]. However, the mechanical properties (tensile strength and stiffness) and water vapour barrier of WPI are reduced [10, 11].

To overcome these characteristics in packaging materials, the addition of nanoparticles has been widely studied [3, 6, 7, 12, 13]. The addition of cellulose nanofibres (CNFs) to biopolymers is an interesting approach because of their low weight, good biodegradability, and renewability as well as the high tensile and puncture strength and reduced water vapour permeability of the formed materials [13–15]. Moreover, the hydrophilicity of CNFs allows their combination with hydrophilic polymers such as WPI [16].

Traditional food packaging is limited in its ability to extend the shelf life of foods [17]. Active packaging is a new concept in food packaging that came with the aim to meet consumer demands and market trends. It can be explained as a type of packaging that increases the shelf life of food

✉ Ana Carolina Salgado de Oliveira
anacarolengalimentos@gmail.com

1 Food Science Department, Federal University of Lavras, Lavras, MG 37200-000, Brazil

2 Chemistry Department, Federal University of Minas Gerais, Belo Horizonte, MG 31270-901, Brazil

products or improves their safety or sensory properties, thus maintaining the quality of the food [18].

Antioxidants are often added to foods that have in its constitution high lipid content in order with the objective of improve their oxidation stability and prolong their life. However, the uncertainty of consumers about the toxicological effects of synthetic antioxidants, even if incorporated into active packaging and not added directly to food, has led to a demand for natural substituents that exhibit antioxidant activity without adding risk to the consumers [19].

Thyme essential oil (TEO) contains the phenolic monoterpenes thymol and carvacrol, which are primarily responsible for its characteristic aroma and antioxidant action [20]. When added to food, TEO is able to prevent oxidation, prolonging the life of the product [21, 22]. However, because of its strong aroma, direct addition of TEO to food products can modify their sensory characteristics, affecting the purchase intent of consumers [23]. Therefore, the addition of TEO to packaging materials may reduce sensory losses caused by direct addition to food products and in turn protect and extend their useful life [24].

Thus, the aim of this study was to evaluate the morphological (scanning electron microscopy), structural (X-ray diffraction and Fourier transformed infrared), thermal (differential scanning calorimetry and thermogravimetric analysis), mechanical (puncture and tensile), water vapour permeability, and optical properties of WPI and CNF bionanocomposites incorporated with different concentrations of TEO.

Material and Methods

Materials

Whey protein isolate (WPI 9400) with 90% of protein was obtained from *Hilmar Ingredients* (Hilmar CA, USA). The glycerol was purchased from Sigma-Aldrich (St. Louis MO, USA). Thyme essential oil (TEO) was obtained from *Ferquima* (Vargem Grande Paulista, SP, Brazil). Cellulose nanofibres (CNFs) were provided by the Department of Forestry—Federal University of Lavras (UFLA, Brazil) and characterized by Bufalino et al. [25]. The CNF had an average diameter of 45 nm and the degree of crystallinity of 58%. Bleached cellulosic pulp from *Eucalyptus* sp.

Experimental Design

The experiment was conducted using a completely randomized design. The concentration of CNFs was set at 4% (w/w) based on the results obtained from preliminary tests [13]. TEO concentrations were 0% (control), 20%, 30%, and 40% (w/w) relative to the base polymer (WPI) and films

were named Control, TEO20, TEO30, and TEO40, respectively. The experiment was conducted in three replicates.

Preparation of Bio-nanocomposite Films

Bio-nanocomposites of WPI and CNFs incorporated with TEO were developed by the *casting* method described by Azevedo et al. [6] with some modifications. WPI and glycerol were fixed at 6% (w/v) in relation to the total volume of the solution and 30% (w/w) relative to the base polymer, respectively. For the production of the control film, WPI was separately dissolved in distilled water in the same way as glycerol and CNFs, and both were kept under stirring for 30 min. Thereafter, the two solutions were mixed and stirred again for 10 min. The pH was adjusted to 8.0 with 1 N NaOH and the final solution was stirred in an ultrasonic homogenizer for the dispersion of nanoparticles (*Branson Sonifier Cell Disruptor* - Model 450D, Manchester, UK) for 10 min with the amplitude of 80% at 25 °C. Subsequently, the solutions were heated at 90 °C for 30 min in a water bath, then cooled and poured on glass plates (18×30 cm^2). For the production of films with TEO, the TEO was added after the filmogenic solution was cooled and followed by again homogenization for 5 min to disperse the TEO for the formation of the emulsion. The solutions remained in the plates for 48 h in order for the solvent to evaporate and for the films to form. The final volume of each solution poured was 125 mL.

Scanning Electron Microscopy (SEM)

Samples for Scanning Electron Microscopy (SEM) were assembled in aluminum double carbon stubs, metalized in a gold evaporator apparatus (SCD 050) and observed in the Scanning Electron Microscope (LEO Evo 40) with an accelerating voltage of 20 kV. The micrographs were obtained from the surface and cross-section of samples cut in liquid nitrogen.

X-ray Diffraction (XRD)

XRD analysis was performed on a *DR-Phaser* diffractometer (Bruker, Karlsruhe, Germany) using a graphite crystal as the monochromator with Cu-kαl ($\lambda = 1.5406$ Å) radiation, operating at 30 kV and 30 mA. Samples were fixed on an aluminium holder and analysed at a scanning rate of 0.02°/s with a 2θ range of 4–50° at 23 °C. The crystallinity index (CI) of bio-nanocomposites was calculated according to Eq. 1 [26]:

$$CI = 1 - \left(I_{min}/I_{max} \right) \times 100 \qquad (1)$$

where CI is the crystallinity index (%), I_{min} is the minimum intensity obtained between the peaks located at 2θ = 9.4° and

$2\theta = 19.4°$, and I_{max} is the maximum intensity of the crystalline peak located at $2\theta = 19.4°$.

Fourier Transformed Infrared (FTIR)

FTIR was performed using an *FTS 3000* spectrometer (Digilab Excalibur, USA) equipped with a KBr detector at a spectral range of 4000–50 cm^{-1}. The number of scans was 64 and the resolution was 4 cm^{-1}.

Thermal Analysis

Differential Scanning Calorimetry (DSC)

DSC measurements were performed using a Shimadzu-DSC60 calorimeter (*Shimadzu Corporation*, Kyoto, Japan). The sample weight ranged from 4–6 mg and the heating rate was 10 °C/min. The following sequence was adopted: (1) the film was first heated from 25 °C to 200 °C in order to eliminate the thermal history (2) the film was cooled from 200 °C to − 50 °C, and (3) the film was then re-heated to 200 °C [27, 28]. From the DSC curves, the glass transition temperature (Tg) was obtained.

Thermogravimetric Analysis (TGA)

The thermal stability and degradation profile of the bionanocomposites were determined by TGA using a Shimadzu-DTG60H (*Shimadzu Corporation*, Kyoto, Japan). The analysis was performed under a nitrogen atmosphere at a flow rate 50 mL/min, with heating from 40 to 500 °C at a rate of 10 °C/min and sample weight of 4–6 mg [29].

Mechanical Properties

Puncture and tensile tests were conducted using a texture analyzer (*Stable Micro Systems*, model TATX2i, UK) with a load cell of 1 kN. For the puncture test, films were cut (9 cm^2) and fixed in an annular ring clamp (diameter of 2.1 cm). A spherical probe with a diameter of 5.0 mm was moved perpendicularly to the film surface at a constant speed of 0.8 mm/s until the probe passed through the film [30]. The puncture strength/thickness (PS) was calculated by dividing the force values at the puncture point by the film thickness to eliminate the thickness variation effect [31], and the deformation (D) values of the films were also determined. The tensile properties were determined according to the standard [32] with the film samples cut into strips (10 × 1.5 cm^2) and the initial separation between the grips was 50 mm with a speed of 0.8 mm/s. The tensile strength (TS, MPa), elongation at break (E), and elastic modulus (EM, MPa) were measured. Five samples of each film in three replicates were used for puncture and strength testing.

Water Vapour Permeability (WVP)

WVP tests were carried out according to Testing, Materials [33] with some modifications. The films were sealed in a permeation cell containing silica gel. The permeation cell was placed in a humidity chamber with a controlled temperature at 23 ± 2 °C, and maintained at 75% relative humidity (RH). The WVP was determined based on the mass of water absorbed by the permeation cell, considering the RH difference between both environments (outside and inside the cell). The samples were weighed for 8 h to a constant weight, and the weight gain values were plotted as a function of time. The slope of each line was calculated by performing a linear regression ($R^2 > 0.9$), and the water vapour transmission rate (WVTR, g/h/m^2) was calculated as the slope of the line divided by the area of the exposed film (m^2). The WVP (g/(m·s·Pa)) was calculated by the following Eq. 2:

$$WVP = (WVTR/\Delta P) \cdot x \qquad (2)$$

where x is the film thickness (mm) and ΔP is the saturation vapour pressure of water (Pa) between the faces of the film: $\Delta P = S (R_1 - R_2)$; S is the saturation vapour pressure at the experimental temperature (2809 kPa), R_1 is the RH outside of the capsule (75%), and R_2 is the RH within the capsule containing silica gel (0%). Five samples of each film in three replicates were used for WVP testing.

Optical Properties

The optical properties of the films were determined using a C-700 spectrophotometric colorimeter (*Konica Minolta*, Japan). The colorimeter was calibrated to white and black standards. Colour CIELab parameters were obtained using D_{65} illumination and observation at 10° in "specular reflectance included" mode. The following parameters were measured: lightness (L^*), intensity of red/green (a^*), intensity of yellow/blue (b^*), and saturation index (c^*). The total color difference (ΔE) of the films was determined by Eq. 3:

$$\Delta E = \sqrt{(L1 - L2) + (a1 - a2) + (b1 - b2)} \qquad (3)$$

where L1 is the initial value of L, a1 is the initial value of a*, b1 is the initial value of b*, L2 is the value of L measured, a2 is the value of a* measured, and b2 is the b* value measured.

The transparency of the films was determined by measuring the percent transmittance (%T) at 600 nm using a spectrophotometer Bel SPECTRO S-200 (Monza, Italy). The transparency (T) was calculated using the following Eq. 4 [34]:

$$T = (Log \%T)/\delta \qquad (4)$$

where δ is the film thickness (mm).

Statistical Analysis

The SEM, DSC, TGA, FTIR, and XRD results were analysed descriptively. The PS, D, RS, E, EM, WVP, and optical properties were analysed using Statistica software (ver. 8, Stat Soft Inc., Tulsa, USA). The analysis of variance test was used and the treatment means were compared by Tukey test.

Results and Discussion

Scanning Electron Microscopy

The surface and cross-section micrographs of incorporated TEO in WPI/CNFs bio-nanocomposites were showed in Figs. 1 and 2.

Bio-nanocomposites of WPI and CNFs without TEO (Control) presented a homogeneous nanoparticle distribution throughout the surface (Fig. 1a) and the cross-section (Fig. 2a) of the sample. However, the addition of TEO interrupted the dispersion of the CNFs (Fig. 1b–d, and Fig. 2b–d). The agglomeration of CNFs may be related to the hydrophobic nature of TEO and hydrophilic nature of CNFs, which reduced the homogeneous interaction of CNFs

throughout the polymeric matrix with a tendency to form bonds among themselves within the agglomeration. The agglomeration could be related too with the disruption of the polymer chains by oil droplets, according to explained by Hosseini et al. [24] when studied the surface of chitosan films incorporated with TEO.

X-ray Diffraction

Figure 3 shows the results of the XRD analysis for WPI/CNFs bio-nanocomposites incorporated TEO. Two peaks of crystallinity were observed at $2\theta = 9.4$ and 19.4 in the films for all samples showing that the addition of TEO did not affect the crystalline structure of the films. This result conforms to Atef et al. [35] which studied the effect of the addition of essential oil in agar- and cellulose-based films and also found no difference in the diffraction structure of the films with the addition of essential oil. The results of crystallinity index (CI) show that the addition of TEO led to an increase in the crystallinity of the bio-nanocomposites. The higher crystallinity values found for the films with added TEO can be explained by the increased interaction between the molecules within the matrix, which limits the movement of the chain and increases the crystallisation
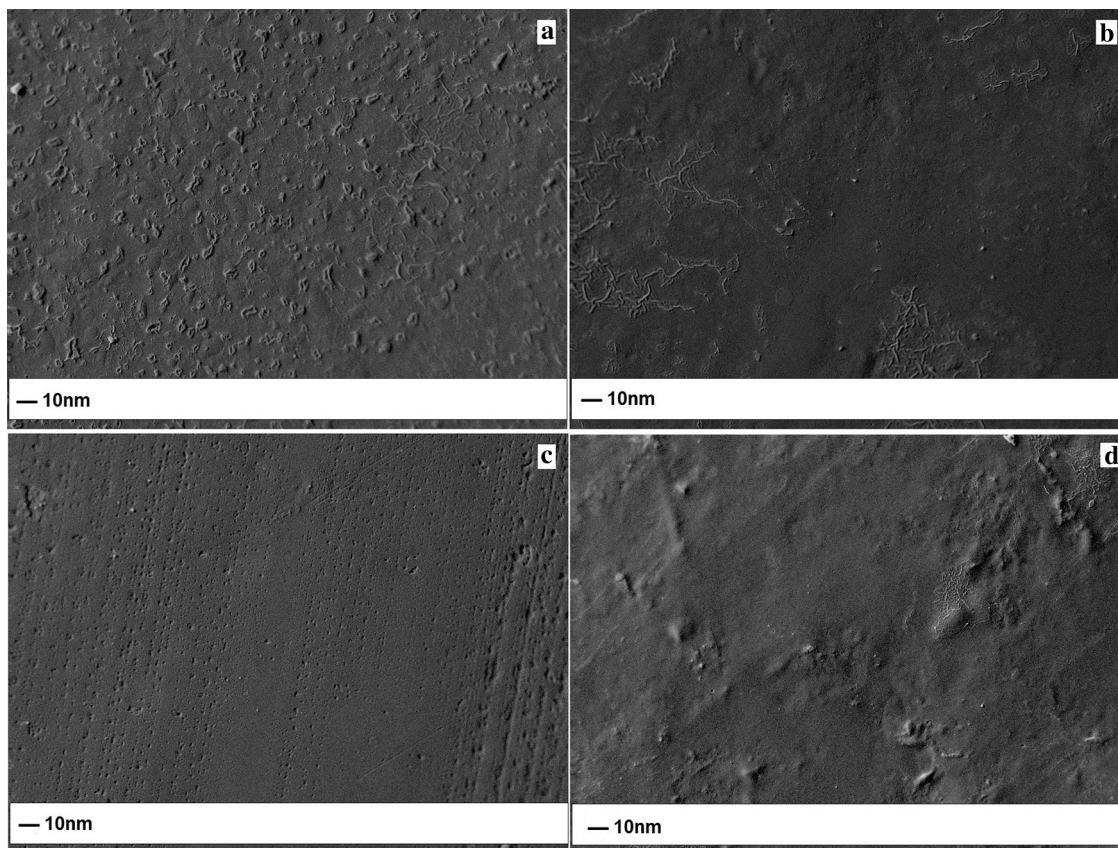

Fig. 1 Surface micrographs of incorporated TEO in WPI/CNFs bio-nanocomposites. 1000 ×. **a** Control; **b** TEO20; **c** TEO30; **d** TEO40
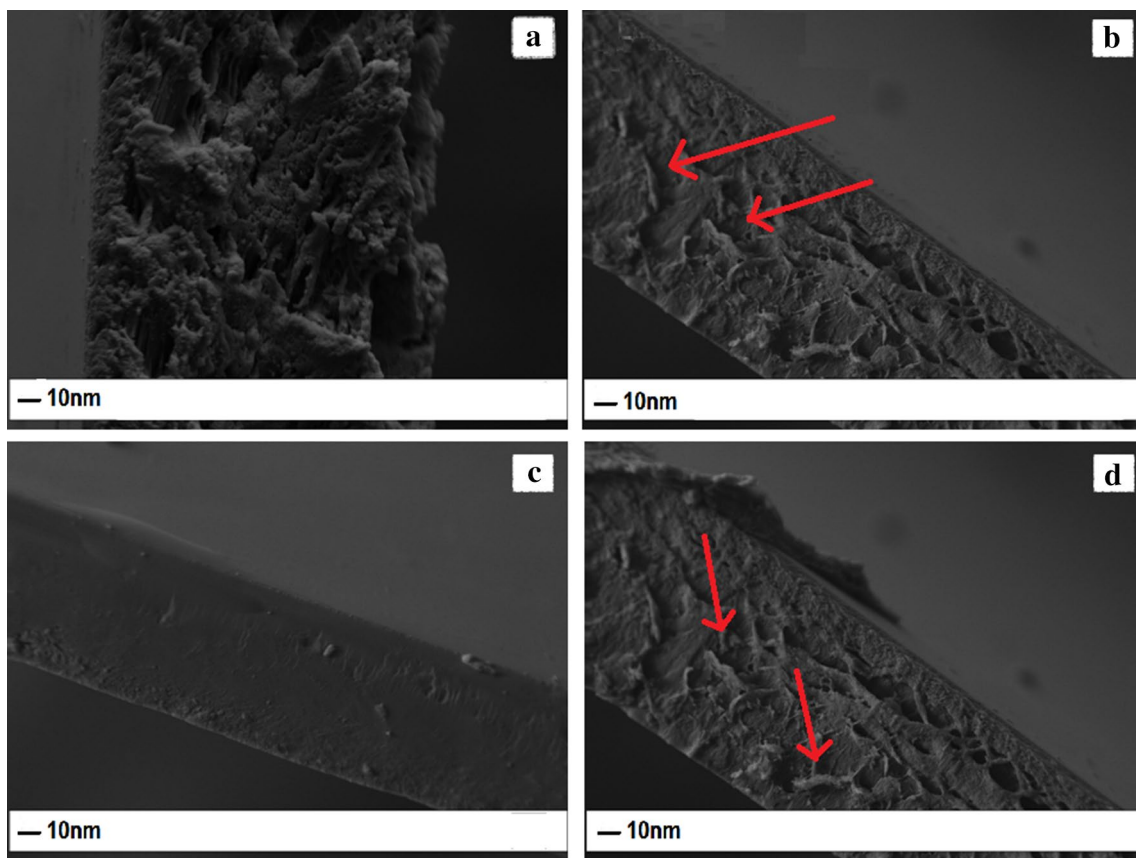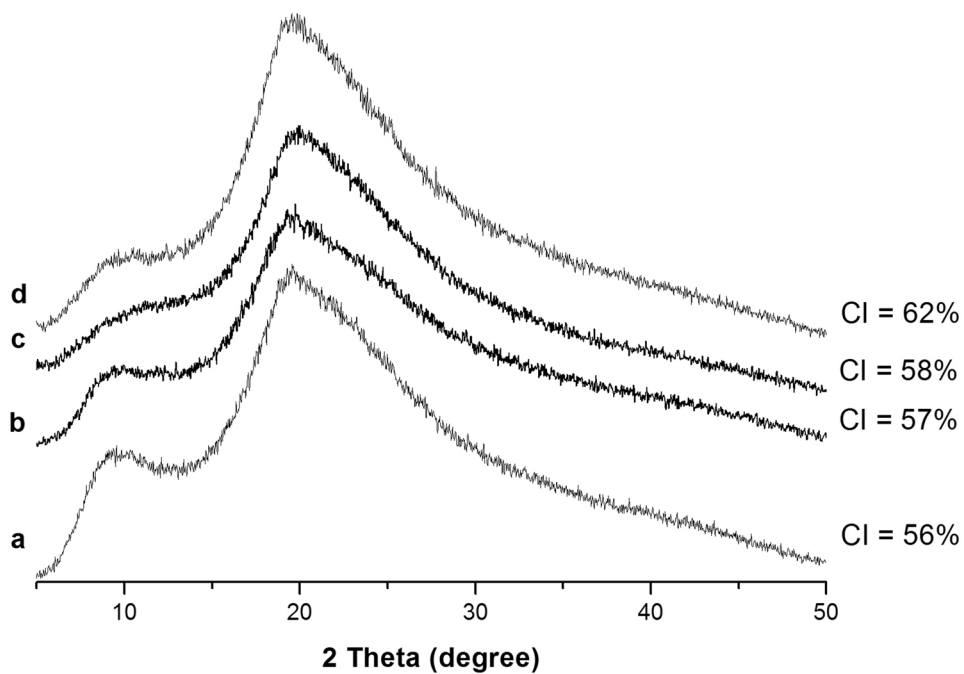
Fig. 2 Cross-section micrographs of incorporated TEO in WPI/CNFs bio-nanocomposites. 1000 ×. **a** Control; **b** TEO20; **c** TEO30; **d** TEO40

Fig. 3 XRD of incorporated TEO in WPI/CNFs bio-nanocomposites. **a** Control; **b** TEO20; **c** TEO40; **d** TEO30

process [36]. Rubilar et al. [37] studied the effect of adding carvacrol and grape seed extract to chitosan films and also found an increase in the percentage of crystallinity index for the films containing carvacrol.

Fourier Transformed Infrared

Figure 4 shows the FTIR results for the samples studied. For all samples, three main absorption peaks were observed in the spectra. The first peak (800–1150 cm^{-1}) is assigned to glycerol and TEO absorption bands, corresponding to the vibrations of C–C and C–O bonds. The second peak (1200–1700 cm^{-1}) is assigned to a combination of vibration of N–H and N–C bonds (1200–1350 cm^{-1}, amide III), N–H bonds (1400–1550 cm^{-1}, amide II), and C = O and N–C (1600–1700 cm^{-1}, amide I) [10]. The regions called amide I and amide II are related to the presence of proteins with secondary structure. Moreover, peaks related to the intermolecular bonds of the β type can be observed at wavelengths of 1612 and 1682 cm^{-1} [38].

The last vibration located in the spectral range of 3000–3600 cm^{-1} was also reported by several authors [10, 39, 40] and is attributed to the stretch band from the OH groups presents in WPI, glycerol, and TEO and free or bound NH. For all treatments, a strong band was observed at 3275 cm^{-1}. Studies demonstrated that the NH stretching band in proteins is usually located at 3254 cm^{-1} [10] and the displacement of the band can be explained, according to Le Tien et al. [39], by the presence of other compounds in the formulation of the films. The CNF is characteristic of a high number of hydroxyl groups capable of binding to other structures and promote displacement of this band.

The first three peaks of spectra also reflect the composition of thyme essential oil consisting primarily of thymol and carvacrol. The band around 800 and 820 cm^{-1} arises from the overlap of the thymol and carvacrol bands. This band can be attributed to off-plane CH vibrations, which are the most important signals used in distinguishing different types of aromatic ring substitution [41]. In addition to these peaks, the peaks at 865 cm^{-1} (C–H out-of-plane beding vibration from isoprenoids), 1116 cm^{-1}, 1175 cm^{-1} (stretching vibrations C–O of mono-, oligo-, and carbohydrate), 1252 cm^{-1} (C–O stretching), 1420 cm^{-1} (C–0 stretching vibrations (amide), and C–C stretching from phenyl groups, COO^{-} symmetric stretching, CH$_2$ bending) [41, 42], 1620 cm^{-1} (aromatic character of terpenes was exhibited by –C = C stretching of benzene ring) [43], and 2950 cm^{-1} (–C–H bonds) [44] reflect the complex composition of this essential oil.

The addition of TEO to bio-nanocomposites of WPI and CNFs did not modify the spectrum without TEO (Fig. 3b–d). This showed the non-interaction between the compounds so that, at the end of the synthesis of the films, the phenolic and active compounds of TEO were still present.

Thermal Analysis

Differential Scanning Calorimetry

The glass transition temperature (Tg) was obtained by DSC analysis. The Tg increased with the addition of TEO to the bio-nanocomposites of WPI and CNFs, featuring more rigid films with stronger bonds (Control: − 14,45 °C; TEO20: − 7,40 °C; TEO30: − 12,78 °C; TEO40: − 9,45 °C). Typically, the Tg increases with increasing chain links, side
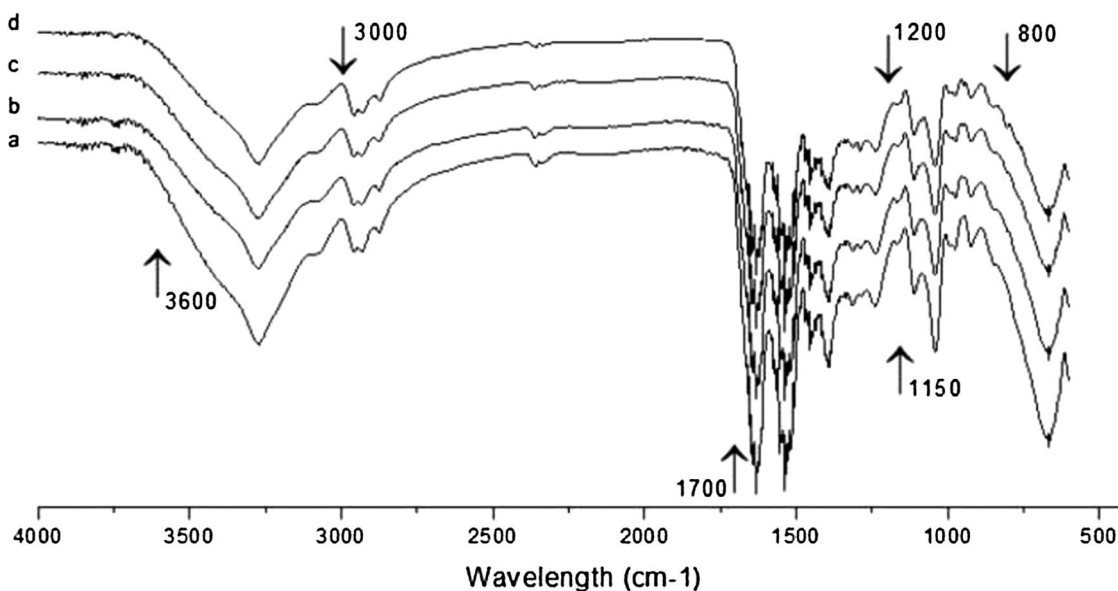

Fig. 4 FTIR spectra of incorporated TEO in WPI/CNFs bio-nanocomposites. **a** Control; **b** TEO20; **c** TEO30; **d** TEO40

groups, crosslinking between the chains, and crystallinity index of the polymer, and decreases with the increase in low molecular weight plasticizers such as water and glycerol [45]. Thus, Tg results are confirmed by XRD results in which increased crystallinity was observed with increasing TEO concentration.

Thermogravimetric Analysis

Through thermogravimetric analysis, Fig. 5 showed two stages of degradation of the bio-nanopolymers in the temperature range of 40 to 500 °C.

The initial degradation peak observed for all treatments was kept close, ranging from 93.2 to 106.8 °C. This first mass reduction indicated the loss of water in the films [46]. The slight decrease in mass at this stage may be related to the incorporation of essential oil in the films [47]. According to Tongnuanchan et al. [48], the essential oil has an effect on mass loss because due to its hydrophobic character can cause a reduction of water diffusion in the films.

A second thermal degradation peak with greater intensity is observed between 160 °C and 380 °C. It is related to the decomposition of the proteins, the use of glycerol as a plasticizer in the formulations, and the degradation of TEO added to the films [46, 49]. The initial degradation temperature (T_i) of the films decreased slightly with the addition of TEO (Table 1), resulting in a reduction of 5.6 °C for the TEO20 treatment compared to the control. The maximum degradation temperature (T_{max}) was obtained from the maximum peaks of degradation from the derivative thermogravimetry (DTG) curves, and the results show a slight increase in the values for the films with added TEO compared to the control. The final degradation temperature (T_f) also showed a slight increase with the addition of TEO, and the percentage of mass loss may be associated with further loss of oil in the films incorporated with TEO [49]. However, the slight increase in T_{max} and T_f did not compromise the thermal stability of the films.

Mechanical Properties

The addition of TEO to nano-biopolymers of WPI and CNFs caused significant differences ($p < 0.05$) to be seen in the results of the puncture test (PS and D) and tensile test (TS, E, and EM), as Table 2. Both tests can be used to measure film hardness [50]. The incorporation of 30% and 40% (w/w) TEO significantly reduced the PS values of the films, as shown in Table 2. The decrease was also observed in the measurements of D, where a progressive reduction with the increase in TEO content was observed. These results showed that the films with TEO were less strong and elastic compared to control.

The properties evaluated by the tensile test (TS, E, and EM) resulted in a reduction in TS and EM only in the film incorporated with the highest concentration of TEO (40% w/w). For E, there was a tendency of decrease for all treatments except for that with 20% (w/w) TEO added, which resulted in a more elastic film compared to others when subjected to strain. These results can be explained by the lack of support and lubrication of the lipids in the polymeric matrix, which may be caused by a partial interruption of the interactions between polymer chains due to the presence

Table 1 Thermal stability of incorporated TEO in WPI/CNFs bio-nanocomposites

Films	T_i* (°C)	$T_{máx}$ (°C)	T_f (°C)	M_{loss} (%) (T_i-T_f)	$Res_{500°C}$ (%)
Control	173.4	302.3	375.3	56.5	22.0
TEO20	167.8	309.7	379.4	57.6	21.7
TEO30	168.6	304.7	380.9	62.1	19.7
TEO40	173.6	308.9	381.8	62.3	18.2

* T_i (initial decomposition temperature); $T_{máx}$ (maximum decomposition temperature); T_f (final decomposition temperature); M_{loss} (mass loss percentage in the decomposition range); $Res_{500°C}$ (percentage of residue at 500 °C)
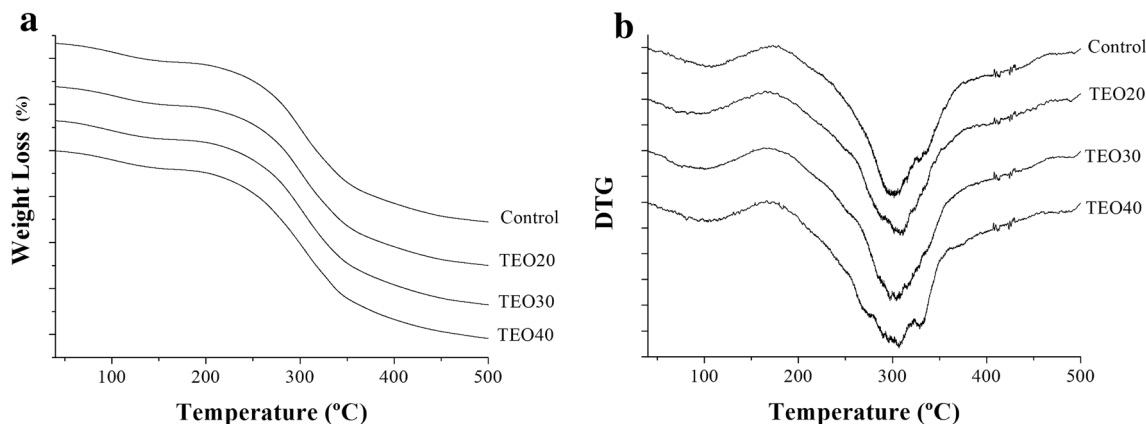

Fig. 5 Weight Loss (%) (**a**) and Derived Thermogravimetry (**b**) curves of incorporated TEO in WPI/CNFs bio-nanocomposites

Table 2 Puncture properties (PS e D) and tesile (TS, E and EM) of incorporated TEO in WPI/CNFs bio-nanocomposites

Films	Puncture strength/thickness (PS) (N/mm)	Puncture deformation (D) (mm)	Tensile strenght (TS) (MPa)	Elongation at break (E) (%)	Elastic Modulus (EM) (MPa)
Control	$87.97^b \pm 3.52$	$3.87^a \pm 1.43$	$6.00^a \pm 0.28$	$22.43^b \pm 1.48$	$45.45^b \pm 2.14$
TEO20	$70.87^b \pm 5.23$	$3.04^b \pm 0.34$	$5.67^a \pm 1.29$	$26.77^a \pm 2.08$	$37.48^b \pm 3.31$
TEO30	$54.19^a \pm 5.57$	$1.69^c \pm 0.71$	$4.86^a \pm 1.04$	$15.69^c \pm 1.19$	$27.00^{ab} \pm 2.95$
TEO40	$40.65^a \pm 3.96$	$1.62^d \pm 0.55$	$3.40^b \pm 0.26$	$13.79^c \pm 0.78$	$13.08^a \pm 1.51$

Means observed in the column with the same letter do not differ statistically ($p < 0.05$)

of non-polar lipid molecules [51], forming non-interactive systems [52]. This fact is proven by the SEM of the samples in this study (Figs. 1, 2) that showed irregularities in the dispersion of CNFs upon the addition of TEO with agglomerations of the nanostructures in the films. This phenomenon resulted in a decreased in mechanical parameters. Moreover, the glass transition temperature (Tg) and crystallinity index increased with the addition and increase of TEO which would lead to an increase in the elastic modulus of the samples. However, this fact was not observed due to irregular CNF dispersion in the TEO addition samples shown in the SEM analysis, decreasing the malleability of the samples.

Water Vapour Permeability

The addition of TEO to the films affected the WVP ($p < 0.05$), as shown in Table 3. A reduction in the WVP values was observed for all treatments compared to the control, with a maximum decrease of 46.2% in the film with the highest concentration of TEO (40% w/w) compared to the control.

The decrease in WVP with increasing concentrations of TEO can be explained by the hydrophobic nature of the oil. WVP usually occurs through the hydrophilic portion of the film and thus, the permeability rate of the material depends on the ratio between the hydrophilic and hydrophobic portions of the components. The increase in the hydrophobic portion of the material forms a barrier to the path of permeation of water vapor molecules, resulting in a lower rate of permeation and WVP [53]. The SEM of the samples in this study (Figs. 1, 2) showed irregularities in the dispersion of CNFs upon the addition of TEO with agglomerations of the nanostructures by the films. This phenomenon could result in increased WVP values by facilitating the passage of water vapor through the points without CNFs. However, the hydrophobic nature of TEO prevailed under the circumstances, as shown through the reduction in WVP. The WVP results are consistent with the results found for the mechanical properties that were also influenced by irregularities in the dispersion of CNFs after the addition of TEO. Furthermore, WPV results are also in line with XDR and Tg results that were influenced by the TEO increment on WPI films.

Table 3 Values of water vapour permeability (WVP) and thickness

Films	WVP $\times 10^{-11}$ (g m^{-1} s^{-1} Pa^{-1})	Thickness (mm)
Control	$6.25^a \pm 0.05$	$0.148^a \pm 0.01$
TEO20	$5.27^b \pm 0.04$	$0.137^b \pm 0.00$
TEO30	$3.43^c \pm 0.05$	$0.137^b \pm 0.01$
TEO40	$3.36^c \pm 0.04$	$0.151^a \pm 0.01$

Means observed in the column with the same letter do not differ statistically ($p < 0.05$)

Optical Properties

The addition of TEO resulted in significant differences ($p < 0.05$) in all optical properties analysed (L^*, a^*, b^*, c^*, ΔE, and transparency) compared to the control, according to Table 4.

For the results of L^*, there was an increase in the film clarity only for the treatment with 30% (w/w) TEO. For a^*, which measures the intensity of red/green colour, the green values increased as the concentration of oil increased, as characterised by the increase in negative values of the parameter. The value of b^*, which measures the intensity of yellow/blue colour, decreased significantly only at the highest concentration of TEO (40% w/w) compared to the other treatments, indicating a decrease in yellow colour for that film. The same result was found for the saturation index (c^*) with a progressive reduction with the increase of TEO, but the reduction was significant only for TEO40, featuring a paler and grey film. The results found for ΔE show that films with 20 and 30% TEO did not show a significant difference for total color difference. ΔE values up to 1.5 are described in the scientific literature as not noticeable by the human eye [54]. TEO40 films have different ΔE values than other samples. However, ΔE values are characterized as "barely noticeable" by the human eye [54]. Thus, for all samples, the total color difference is small relative to the control.

The value of the transparency of WPI and CNF bio-nanocomposites with TEO added was reduced as the concentration of TEO increased. This result was probably due to oil that was dispersed throughout the matrix protein and the

Table 4 Colour parameters (L^*, a^*, b^*, C^*, ΔE, T)

Films	L^*	a^*	b^*	C^*	ΔE	T(log(%T)/mm)
Control	$88.31^a \pm 0.11$	$-0.08a \pm 0.05$	$2.21^a \pm 0.24$	$2.21^a \pm 0.23$	–	$14.15^a \pm 0.85$
TEO20	$88.33^a \pm 0.05$	$-0.27^b \pm 0.02$	$1.68^b \pm 0.04$	$1.70^b \pm 0.03$	$0.56^a \pm 0.02$	$13.10^b \pm 0.65$
TEO30	$88.66^b \pm 0.05$	$-0.38^b \pm 0.05$	$1.87^{ab} \pm 0.02$	$1.90^{ab} \pm 0.03$	$0.57^a \pm 0.03$	$13.74^b \pm 0.80$
TEO40	$88.37a \pm 0.03$	$-0.67^c \pm 0.03$	$0.38^c \pm 0.12$	$0.77^c \pm 0.08$	$1.92^b \pm 0.05$	$11.68^c \pm 0.18$

Means observed in the column with the same letter do not differ statistically ($p < 0.05$)

increased volume of emulsion in the film solution, consequently increasing the opacity and reducing the transparency. Moreover, this result is also related to the crystallinity index of the material. Crystalline materials try to be more opaque and amorphous materials try to be more transparent. The crystalline regions reflect or deflect the beam of the incident light, compromising the transmission of light, which provides greater opacity [55]. In this study, the addition of TEO to the films increased the crystallinity index of the samples, thus decreasing the transparency.

Conclusions

The addition of TEO to bio-nanocomposites of WPI and CNFs, in the concentration range tested, enabled the formation of materials with positive results for WVP, thermal stability, and crystallinity index of the films. Moreover, films with TEO added became less yellow (b*), tended to green (a*), and were paler (c*) and less transparent. The mechanical properties were reduced creating films that were less rigid and elastic. SEM showed a decrease in CNF dispersion with the incorporation of TEO. In addition, the mechanical properties showed the formation of non-interactive systems and the FTIR spectra showed maintenance of the phenolic compounds of the TEO after the synthesis of the films. The addition of TEO in WPI/CNF films resulted in a material with morphological, mechanical, barrier and optical properties that encourage the studies for various applications.

References

1. Felix M, Perez-Puyana V, Romero A, Guerrero A (2017) Production and characterization of bioplastics obtained by injection moulding of various protein systems. J Polym Environ 25(1):91–100. https://doi.org/10.1007/s10924-016-0790-7
2. Li J, Chen H (2000) Biodegradation of whey protein-based edible films. J Polym Environ 8(3):135–143. https://doi.org/10.1023/a:1014877800102
3. Oymaci P, Altinkaya SA (2016) Improvement of barrier and mechanical properties of whey protein isolate based food packaging films by incorporation of zein nanoparticles as a novel bio-nanocomposite. Food Hydrocoll 54:1–9. https://doi.org/10.1016/j.foodhyd.2015.08.030
4. Reis AB, Yoshida CM, Reis APC, Franco TT (2011) Application of chitosan emulsion as a coating on Kraft paper. Polym Int 60(6):963–969. https://doi.org/10.1002/pi.3023
5. Siracusa V, Rocculi P, Romani S, Dalla Rosa M (2008) Biodegradable polymers for food packaging: a review. Trends Food Sci Technol 19(12):634–643. https://doi.org/10.1016/j.tifs.2008.07.003
6. Azevedo VM, Dias MV, Borges SV, Costa ALR, Silva EK, Medeiros ÉAA, Nilda de Fátima FS (2015) Development of whey protein isolate bio-nanocomposites: effect of montmorillonite and citric acid on structural, thermal, morphological and mechanical properties. Food Hydrocoll 48:179–188. https://doi.org/10.1016/j.foodhyd.2015.02.014
7. Azevedo VM, Dias MV, Siqueira Elias de HH, Fukushima KL, Silva EK, de Deus Souza Carneiro J, de Fátima Ferreira Soares N, Borges SV (2018) Effect of whey protein isolate films incorporated with montmorillonite and citric acid on the preservation of fresh-cut apples. Food Res Int 107:306–313. https://doi.org/10.1016/j.foodres.2018.02.050
8. Hong S-I, Krochta JM (2006) Oxygen barrier performance of whey-protein-coated plastic films as affected by temperature, relative humidity, base film and protein type. J Food Eng 77(3):739–745. https://doi.org/10.1016/j.jfoodeng.2005.07.034
9. Garrido Assis OB, de Britto D (2011) Evaluation of the antifungal properties of chitosan coating on cut apples using a non-invasive image analysis technique. Polym Int 60(6):932–936. https://doi.org/10.1002/pi.3039
10. Ramos ÓL, Reinas I, Silva SI, Fernandes JC, Cerqueira MA, Pereira RN, Vicente AA, Poças MF, Pintado ME, Malcata FX (2013) Effect of whey protein purity and glycerol content upon physical properties of edible films manufactured therefrom. Food Hydrocoll 30(1):110–122. https://doi.org/10.1016/j.foodhyd.2012.05.001
11. Gällstedt M, Hedenqvist MS (2002) Oxygen and water barrier properties of coated whey protein and chitosan films. J Polym Environ 10(1):1–4. https://doi.org/10.1023/a:1021068304169
12. Aulin C, Gällstedt M, Lindström T (2010) Oxygen and oil barrier properties of microfibrillated cellulose films and coatings. Cellulose 17(3):559–574. https://doi.org/10.1007/s10570-009-9393-y

13. Carvalho RA, Santos TA, de Azevedo VM, Felix PHC, Dias MV, Borges SV (2018) Bio-nanocomposites for food packaging applications: effect of cellulose nanofibers on morphological, mechanical, optical and barrier properties. Polym Int 67(4):386–392. https://doi.org/10.1002/pi.5518

14. Sanchez-Garcia M, Lagaron J (2010) On the use of plant cellulose nanowhiskers to enhance the barrier properties of polylactic acid. Cellulose 17(5):987–1004. https://doi.org/10.1007/s10570-010-9430-x

15. Spence KL, Venditti RA, Rojas OJ, Habibi Y, Pawlak JJ (2010) The effect of chemical composition on microfibrillar cellulose films from wood pulps: water interactions and physical properties for packaging applications. Cellulose 17(4):835–848. https://doi.org/10.1007/s10570-010-9424-8

16. Siro I, Plackett D (2010) Microfibrillated cellulose and new nanocomposite materials: a review. Cellulose 17(3):459–494. https://doi.org/10.1007/s10570-010-9405-y

17. Dainelli D, Gontard N, Spyropoulos D, Zondervan-van den Beuken E, Tobback P (2008) Active and intelligent food packaging: legal aspects and safety concerns. Trends Food Sci Technol 19:S103–S112. https://doi.org/10.1016/j.tifs.2008.09.011

18. Soares NDFF, da Silva WA, dos Santos Pires AC, Camilloto GP, Silva PS (2015) Novos desenvolvimentos e aplicações em embalagens de alimentos. Ceres 56(4).

19. Siripatrawan U, Harte BR (2010) Physical properties and antioxidant activity of an active film from chitosan incorporated with green tea extract. Food Hydrocoll 24(8):770–775. https://doi.org/10.1016/j.foodhyd.2010.04.003

20. Yanishlieva NV, Marinova E, Pokorný J (2006) Natural antioxidants from herbs and spices. European J Lipid Sci Technol 108(9):776–793. https://doi.org/10.1002/ejlt.200600127

21. Fratianni F, De Martino L, Melone A, De Feo V, Coppola R, Nazzaro F (2010) Preservation of chicken breast meat treated with thyme and balm essential oils. J Food Sci 75(8):M528–M535. https://doi.org/10.1111/j.1750-3841.2010.01791.x

22. Tomaino A, Cimino F, Zimbalatti V, Venuti V, Sulfaro V, De Pasquale A, Saija A (2005) Influence of heating on antioxidant activity and the chemical composition of some spice essential oils. Food Chem 89(4):549–554. https://doi.org/10.1016/j.foodchem.2004.03.011

23. Scollard J, Francis GA, O'Beirne D (2013) Some conventional and latent anti-listerial effects of essential oils, herbs, carrot and cabbage in fresh-cut vegetable systems. Postharvest Biol Technol 77:87–93. https://doi.org/10.1016/j.postharvbio.2012.11.011

24. Hosseini MH, Razavi SH, Mousavi MA (2009) Antimicrobial, physical and mechanical properties of chitosan-based films incorporated with thyme, clove and cinnamon essential oils. J Food Process Preserv 33(6):727–743. https://doi.org/10.1111/j.1745-4549.2008.00307.x

25. Bufalino L, de Sena Neto AR, Tonoli GHD, de Souza FA, Costa TG, Marconcini JM, Colodette JL, Labory CRG, Mendes LM (2015) How the chemical nature of Brazilian hardwoods affects nanofibrillation of cellulose fibers and film optical quality. Cellulose 22(6):3657–3672. https://doi.org/10.1007/s10570-015-0771-3

26. Segal L, Creely JJ, Martin AE, Conrad CM (1959) An empirical method for estimating the degree of crystallinity of native cellulose using the x-ray diffractometer. Text Res J 29(10):786–794. https://doi.org/10.1177/004051755902901003

27. ASTM D (1999) 3417–99. Standard test method for enthalpies of fusion and crystallization of polymers by differential scanning calorimetry (DSC). Conshohocken, Annual Book of ASTM Standards, p 02

28. ASTM A (2003) D3418–03 Standard test method for transition temperatures and enthalpies of fusion and crystallization of polymers by differential scanning calorimetry. West Conshohocken, ASTM International

29. Jones A, Mandal A, Sharma S (2015) Protein-based bioplastics and their antibacterial potential. J Appl Polym Sci. https://doi.org/10.1002/app.41931

30. ASTM Standard test method for slow rate penetration resistance of flexible barrier films and laminates. In 1990. American Society for Testing and Materials

31. Park S-i, Zhao Y (2004) Incorporation of a high concentration of mineral or vitamin into chitosan-based films. J Agric Food Chem 52(7):1933–1939. https://doi.org/10.1021/jf034612p

32. ASTM D (2002) Standard test method for tensile properties of thin plastic sheeting. vol 14. West Conshohocken, ASTM International (EUA)

33. Testing ASf, Materials (2013) Standard test methods for water vapor transmission of materials. West Conshohocken, ASTM International

34. ASTM (1980) Standard test method for transparency of plastic sheeting. Conshohocken, Annual Book of ASTM Standards

35. Atef M, Rezaei M, Behrooz R (2014) Preparation and characterization agar-based nanocomposite film reinforced by nanocrystalline cellulose. Int J Biol Macromol 70:537–544. https://doi.org/10.1016/j.ijbiomac.2014.07.013

36. Cerqueira MA, Souza BWS, Teixeira JA, Vicente AA (2012) Effect of glycerol and corn oil on physicochemical properties of polysaccharide films—a comparative study. Food Hydrocoll 27(1):175–184. https://doi.org/10.1016/j.foodhyd.2011.07.007

37. Rubilar JF, Cruz RMS, Silva HD, Vicente AA, Khmelinskii I, Vieira MC (2013) Physico-mechanical properties of chitosan films with carvacrol and grape seed extract. J Food Eng 115(4):466–474. https://doi.org/10.1016/j.jfoodeng.2012.07.009

38. Hammann F, Schmid M (2014) Determination and quantification of molecular interactions in protein films: a review. Materials 7(12):7975–7996. https://doi.org/10.3390/ma7127975

39. Le Tien C, Letendre M, Ispas-Szabo P, Mateescu MA, Delmas-Patterson G, Yu HL, Lacroix M (2000) Development of biodegradable films from whey proteins by cross-linking and entrapment in cellulose. J Agric Food Chem 48(11):5566–5575. https://doi.org/10.1021/jf0002241

40. Jutrzenka Trzebiatowska P, Dzierbicka A, Kamińska N, Datta J (2018) The influence of different glycerine purities on chemical recycling process of polyurethane waste and resulting semi-products. Polym Int 67(10):1368–1377. https://doi.org/10.1002/pi.5638

41. Lin-Vien D, Colthup NB, Fateley WG, Grasselli JG (1991) The handbook of infrared and Raman characteristic frequencies of organic molecules. Elsevier, Amsterdam

42. Topala CM, Tataru LD (2016) ATR-FTIR Study of thyme and rosemary oils extracted by supercritical carbon dioxide. Rev Chim (Bucharest) 67:842–846

43. Scacchetti FAP, Pinto E, Soares GMB (2017) Functionalization and characterization of cotton with phase change materials and thyme oil encapsulated in beta-cyclodextrins. Prog Org Coat 107:64–74. https://doi.org/10.1016/j.porgcoat.2017.03.015

44. Chung SK, Seo JY, Lim JH, Park HH, Yea MJ, Park HJ (2013) Microencapsulation of essential oil for insect repellent in food packaging system. J Food Sci 78(5):E709–E714. https://doi.org/10.1111/1750-3841.12111

45. Galietta G, Di Gioia L, Guilbert S, Cuq B (1998) Mechanical and thermomechanical properties of films based on whey proteins as affected by plasticizer and crosslinking agents. J Dairy Sci 81(12):3123–3130. https://doi.org/10.3168/jds.S0022-0302(98)75877-1

46. Kadam DM, Thunga M, Wang S, Kessler MR, Grewell D, Lamsal B, Yu C (2013) Preparation and characterization of whey protein isolate films reinforced with porous silica coated

titania nanoparticles. J Food Eng 117(1):133–140. https://doi.org/10.1016/j.jfoodeng.2013.01.046

47. Mondal D, Bhowmick B, Mollick MMR, Maity D, Mukhopadhyay A, Rana D, Chattopadhyay D (2013) Effect of clay concentration on morphology and properties of hydroxypropylmethylcellulose films. Carbohydr Polym 96(1):57–63. https://doi.org/10.1016/j.carbpol.2013.03.064

48. Tongnuanchan P, Benjakul S, Prodpran T (2011) Roles of lipid oxidation and pH on properties and yellow discolouration during storage of film from red tilapia (*Oreochromis niloticus*) muscle protein. Food Hydrocoll 25(3):426–433. https://doi.org/10.1016/j.foodhyd.2010.07.013

49. Basiak E, Debeaufort F, Lenart A (2016) Effect of oil lamination between plasticized starch layers on film properties. Food Chem 195:56–63. https://doi.org/10.1016/j.foodchem.2015.04.098

50. Arvanitoyannis I (2005) Food packaging technology. Edited by R Coles, D McDowell and MJ Kirwan. Blackwell Publishing, CRC Press, Oxford, 2003. 346 pp ISBN 0-8493-97788-X. J Sci Food Agric 85(6):1072–1072. https://doi.org/10.1002/jsfa.2089

51. Liu L, Kerry JF, Kerry JP (2006) Effect of food ingredients and selected lipids on the physical properties of extruded edible films/casings. Int J Food Sci Technol 41(3):295–302. https://doi.org/10.1111/j.1365-2621.2005.01063.x

52. Mor Y, Shoemaker CF, Rosenberg M (1999) Compressive properties of whey protein composite gels containing fractionated Milkfat. J Food Sci 64(6):1078–1083. https://doi.org/10.1111/j.1365-2621.1999.tb12286.x

53. Garcia MA, Martino MN, Zaritzky NE (2000) Lipid addition to improve barrier properties of edible starch-based films and coatings. J Food Sci 65(6):941–947. https://doi.org/10.1111/j.1365-2621.2000.tb09397.x

54. Ramos E, Gomide L (2017) Avaliação da Qualidade de Carnes: Fundamentos e Metodologias (ed.). Viçosa: Editora UFV

55. Sarantópoulos C, Oliveira LD, Padula M, Coltro L, Alves RM, Garcia EE (2002) Embalagens plásticas flexíveis: principais polímeros e avaliação de propriedades. Campinas: CETEA/ITAL 1:267